ARTICLE

Heterogeneous functional state dynamics and its structural substrates in male individuals with autism spectrum disorder

Tianhang Liu[1], Xi Chen[1], Xiangyu Zheng[2,3], Haoda Ren[1], Yapei Xie[4,5,6], Zhao Fu[2], Yilu Zhao[2], Li Yang[2]✉, Yong He[4,5,6,7]✉ and Xuhong Liao[1,5]✉

Neuroimaging studies have revealed altered functional connectome dynamics in autism spectrum disorder (ASD) and linked these alterations to clinical symptoms. However, most studies have emphasized population-level contrasts, leaving interindividual variability in connectome dynamics and its structural underpinnings poorly understood. To address this gap, we analyzed resting-state functional and structural MRI data from 939 male participants (440 with ASD, 499 typically developing controls) across 18 sites in the Autism Brain Imaging Data Exchange (ABIDE). Whole-brain functional state dynamics was characterized using five leading activity modes and their expressions via eigen-microstate analysis. Age-related trajectories of mode expressions were constructed for typically developing controls using normative modeling, enabling quantification of individual-level deviations in functional dynamics. Compared with controls, ASD individuals showed greater interindividual variability in functional deviation profiles. Unsupervised clustering of these profiles identified two robust ASD subtypes with distinct mode-specific dysfunctions. One subtype primarily involved the visual, default-mode, frontoparietal, and dorsal attention networks, whereas the other subtype primarily involved the somatomotor, visual, frontoparietal, and ventral attention networks. These subtypes were clinically dissociable, differing in restricted and repetitive behaviors and social impairments, and exhibited mode-specific brain-symptom associations. Furthermore, the subtypes exhibited distinct cortical thickness alterations, and individual subtype membership was predicted with high accuracy (83%) using a random forest classifier based on cortical thickness. The main findings were replicated in an independent cohort outside ABIDE. This study delineates two reproducible and clinically dissociable ASD subtypes and links functional connectome dynamics to structural substrates, offering novel insights into the neurobiological basis behind ASD heterogeneity.

Molecular Psychiatry; https://doi.org/10.1038/s41380-026-03627-y

INTRODUCTION

Autism spectrum disorder (ASD) is a neurodevelopmental condition characterized by profound clinical and neurobiological heterogeneity [1, 2]. This heterogeneity complicates efforts to uncover its mechanisms and improve diagnosis. Contemporary perspectives conceptualize autism as a disconnection syndrome, characterized by widespread disruptions in functional connectivity organization, particularly in the default-mode and somatomotor networks [3, 4]. Recently, increasing attention has shifted towards functional connectome dynamics, which tracks time-resolved reconfigurations of brain networks supporting cognitive flexibility and adaptive behavior [5–7]. Altered connectome dynamics have been observed in ASD, including increased connectivity variability [8, 9], aberrant intermodular switching [10], and reduced functional state transitions [11–13]. These findings indicate disrupted dynamic coordination and impaired neural flexibility in ASD. Importantly, beyond temporally aggregated measures, functional state dynamics capture the transient and metastable nature of whole-brain functional configurations [14]. This state-resolved perspective allows identification of disease-related alterations and clinical associations specific to certain functional states [12, 13], thereby potentially offering sensitive and specific markers of pathology and behavior in ASD [14, 15].

Most prior studies, however, have focused on population-level contrasts in connectome dynamics, largely overlooking interindividual variability. Given the substantial heterogeneity of ASD, it is critical to move beyond case-control designs and toward individualized characterization of functional deviations [16–18]. Such an approach is essential for precision diagnosis and intervention [19–21]. Only a few studies have attempted to address this gap [22–24], but limitations remain. Two studies focused narrowly on dynamic configurations of the salience network [22, 23]. Another study combined static and dynamic connectivity measures (mean and variability) for subtyping, yet

[1]School of Systems Science, Beijing Normal University, Beijing, China. [2]Peking University Sixth Hospital, Peking University Institute of Mental Health, Beijing Key Laboratory for Big Data Innovative Application of Child and Adolescent Mental Disorders, National Clinical Research Center for Mental Disorders (Peking University Sixth Hospital), NHC Key Laboratory of Mental Health (Peking University), Beijing, China. [3]Department of Child and Adolescent Psychiatry, Shanghai Mental Health Center, Shanghai Jiao Tong University School of Medicine, Shanghai, China. [4]State Key Laboratory of Cognitive Neuroscience and Learning, Beijing Normal University, Beijing, China. [5]Beijing Key Laboratory of Brain Imaging and Connectomics, Beijing Normal University, Beijing, China. [6]IDG/McGovern Institute for Brain Research, Beijing Normal University, Beijing, China. [7]Chinese Institute for Brain Research, Beijing, China. ✉email: yangli_pkuimh@bjmu.edu.cn; yong.he@bnu.edu.cn; liaoxuhong@bnu.edu.cn

Received: 18 September 2025 Revised: 1 April 2026 Accepted: 17 April 2026
Published online: 02 May 2026

the resulting subgroups exhibited highly overlapping clinical profiles [24]. These approaches have ignored transient whole-brain functional states, which may capture subtle, disease-related functional alterations and clinically relevant associations [14, 15]. Moreover, the structural substrates underlying individual variability in functional dynamics remain largely unexplored. Brain anatomy provides the fundamental scaffold for functional organization [25]. Accumulating evidence suggests that functional connectome dynamics is constrained by multiple anatomical factors, including the strength and modular organization of white-matter connectivity [9, 26, 27] and the hierarchical organization of the cortex [28]. Recent work has further demonstrated a tight coupling between interindividual differences in functional and structural connectivity [29]. However, how anatomical features contribute to heterogeneous connectome dynamics in ASD remains unclear.

To address this gap, we integrated whole-brain functional state dynamics with normative modeling to quantify individual-level deviations in ASD and to examine their structural substrates. Normative modeling provides a robust statistical framework for estimating subject-specific deviations from normative trajectories, while accounting for age-related effects [30–33]. Specifically, we leveraged resting-state functional and structural MRI data from a large multisite cohort of 939 male participants from the Autism Brain Imaging Data Exchange (ABIDE) [34, 35]. Using eigen-microstate analysis of functional data [36–38], we derived a low-dimensional representation of functional state dynamics, which captures metastable functional states and their temporal expressions [38]. We then assessed heterogeneity in individual deviation profiles of functional state dynamics and clustered these profiles to identify reproducible ASD subtypes. Finally, we compared these subtypes in terms of connectome dynamics alterations, association with clinical symptoms, and cortical thickness differences. The generalizability of the main findings was evaluated using an independent dataset outside ABIDE. We hypothesized that (1) individuals with ASD would exhibit heterogeneous deviations in functional state dynamics, giving rise to reproducible neurophysiological subtypes with distinct clinical profiles; and (2) these subtypes would be associated with underlying anatomical substrates. Here, we focused on cortical thickness as the structural measure, given that cortical thickness alterations have been frequently reported in ASD [39–41].

METHODS AND MATERIALS

Participants

Two datasets were used here, including the publicly available ABIDE dataset [34, 35] and an independent cohort from Peking University Sixth Hospital (PKUSH). The ABIDE dataset was used for the main discovery, whereas the PKUSH dataset served as an independent validation cohort.

ABIDE discovery cohort. We used resting-state functional MRI (rs-fMRI) and structural MRI (sMRI) data from 939 male participants (440 with ASD and 499 typically developing (TD) controls; aged 5-35 years) across 18 independent sites from ABIDE I and II datasets (https://fcon_1000.projects.nitrc.org/indi/abide/) [34, 35]. Data were screened using stringent criteria [10], considering sex, structural image quality, rs-fMRI scanning protocols, head motion, brain coverage, spatial normalization, full-scale intelligence quotient (FSIQ), and age range (Supplement). Clinical assessments included the Autism Diagnostic Interview-Revised (ADI-R), the Autism Diagnostic Observation Schedule-Second Edition (ADOS-2), and the Social Responsiveness Scale (SRS).

PKUSH validation cohort. We used functional and structural data from 90 male participants (42 with ASD and 48 TD controls; aged 6-17 years), selected using the same screening criteria as the ABIDE cohort (Supplement). Clinical assessments included ADOS-2.

The ABIDE dataset is publicly available, and details of data acquisition and ethical approval can be found in the original publications [34, 35]. The PKUSH dataset was approved by the Ethics Committee of Peking University Sixth Hospital (Approval No. 2023-61). All methods were performed in accordance with the relevant guidelines and regulations. Demographic information for all participants and clinical characteristics for individuals with ASD are summarized in Table 1 and Tables S1-S2.

Data preprocessing

All rs-fMRI and sMRI data from both cohorts were preprocessed using harmonized pipelines, implemented with the GRETNA package [42] and the Computational Anatomy Toolbox (CAT12) [43], respectively (Supplement). For rs-fMRI, preprocessing included removal of the first 10-second volumes, slice timing correction, realignment, spatial normalization to the Montreal Neurological Institute (MNI) standard space, spatial smoothing with an isotropic 6-mm full-width at half-maximum Gaussian kernel, linear detrending, nuisance regression, and temporal band-pass filtering (0.01-0.1 Hz). Structural data were preprocessed with bias-field inhomogeneity correction, skull stripping, and spatial normalization to MNI space [44]. The resulting probability maps of gray matter, white matter, and cerebrospinal fluid were then used for subsequent brain morphology analyses.

Analyzing functional state dynamics of spontaneous brain activity

To characterize functional state dynamics, we applied eigen-microstate analysis to rs-fMRI data from the TD group to identify a set of leading activity modes and their corresponding coactivation patterns [38] (Supplement). These leading activity modes capture recurrent and dominant patterns of whole-brain functional activity underlying spontaneous fluctuations.

Analyses were performed at the node level using a prior functional parcellation of 1000 cortical nodes [45], which allowed us to capture

Table 1. Demographic characteristics of participants.

	ASD	TD	*p* Value
ABIDE cohort	$n = 440$	$n = 499$	
Age, years	5.32-34.46 (14.28 ± 5.38)	5.89-34.05 (14.35 ± 5.37)	0.843
FSIQ	71-149 (107.07 ± 16.61)	73-148 (112.81 ± 12.92)	<0.001***
Mean FD, mm	0.04-0.50 (0.20 ± 0.10)	0.04-0.49 (0.18 ± 0.09)	<0.001***
PKUSH cohort	$n = 42$	$n = 48$	
Age, years	6.75-17.00 (10.25 ± 2.68)	6.83-13.08 (9.74 ± 1.75)	0.282
FSIQ	76-134 (101.93 ± 16.03)	96-150 (117.13 ± 12.29)	<0.001***
Mean FD, mm	0.07-0.49 (0.24 ± 0.12)	0.07-0.37 (0.18 ± 0.08)	0.013*

All values are presented as range (mean ± SD).
All *p* values were obtained from two-sample t-tests; *$p < 0.05$; ***$p < 0.001$.
ASD autism spectrum disorder, *TD* typically developing, *ABIDE* autism brain imaging data exchange, *PKUSH* peking university sixth hospital, *SD* standard deviation, *FSIQ* full-scale intelligence quotient, *Mean FD* mean framewise displacement.

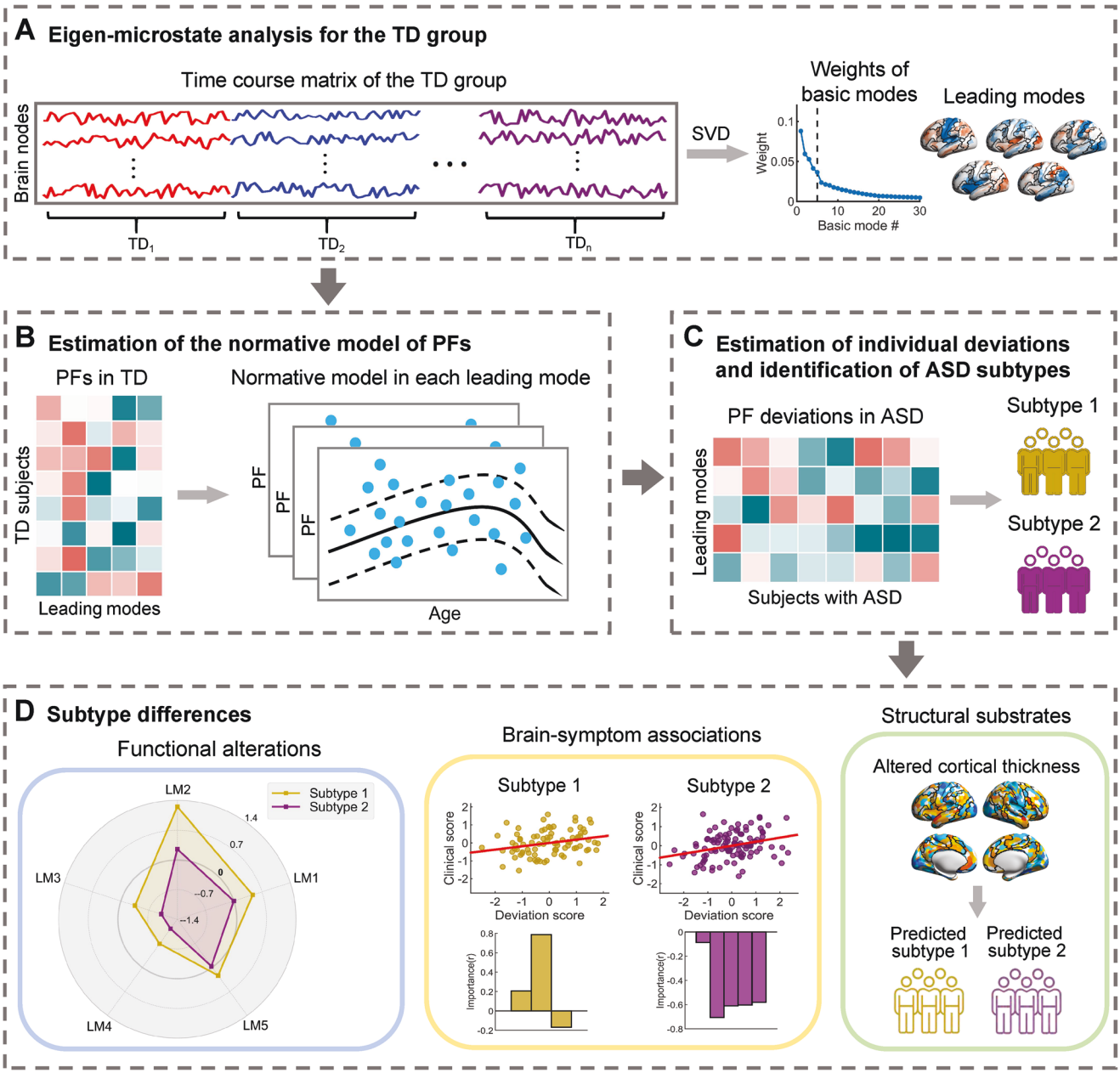

Fig. 1 Flowchart of data analysis. A Eigen-microstate analysis of group-level time courses from typically developing controls. Five leading modes were identified based on the weight curve, representing dominant and recurring functional activity patterns at rest. **B** Normative modeling of projection feature (PF) values for each leading mode. Models were trained in the typically developing group, using Gaussian process regression (blue dots). The solid line denotes the predicted age-related trajectory of PFs, and dashed lines denote the normative range. **C** Estimation of individual PF deviations from the normative models and identification of autism spectrum disorder subtypes based on these deviations. **D** Multidimensional subtype differences, including alterations in functional profiles, brain-symptom associations, and structural substrates. Individual subtype membership was predicted using altered cortical thickness features. Cortical maps were visualized on the brain surface using BrainNet Viewer [99]. ASD autism spectrum disorder, TD typically developing, SVD singular value decomposition, LM leading mode.

whole-brain dynamics while reducing computational complexity. For each participant, nodal time courses were extracted and standardized. Data from TD individuals were concatenated to construct a group-level representation of functional activity, namely, matrix ***A***. ComBat harmonization [46] was applied to matrix ***A*** to mitigate site-related effects while retaining age, FSIQ, and mean framewise displacement (FD) as regressors to preserve biologically meaningful variability [47]. Leading activity modes were then derived from the harmonized group-level matrix ***A*** using singular value decomposition (SVD) (Fig. 1A; Supplement). These modes, referred to as dominant eigen-microstates, can be viewed as fundamental building blocks of large-scale functional dynamics. The number of leading modes was determined based on the spectral properties of the mode weights, capturing the transition from dominant to negligible contributions (Supplement). Five leading modes were identified in the TD group (i.e., $K = 5$; Fig. S1), corresponding to the last mode preceding the knee point in the ordered spectrum of mode weights. This knee point, reflecting a pronounced drop in weights according to Cattell's scree criterion [48], was objectively detected using the kneedle algorithm [49].

For each leading mode, we further characterized its corresponding coactivation pattern (Supplement). Brain regions with the same sign of activity amplitude indicate positive coactivation, whereas regions with opposite signs indicate anti-coactivation. Coactivation patterns were

further summarized at the system level based on seven predefined functional systems [50] to explore the functional system dependence.

We next quantified individual-level functional state dynamics by analyzing the temporal expressions of the identified leading modes in both TD and ASD participants. For each participant, the expression strength of each mode was defined as a projection feature (PF), reflecting the degree to which a given functional mode was expressed over time (Supplement).

To reduce potential confounds related to site-specific scan length, we adopted a resampling strategy in which a fixed number of time points were randomly selected for each participant to construct matrix ***A***. This procedure was repeated multiple times (i.e., 100 times), and mode expression measures were averaged across repetitions to obtain stable estimates. The influence of the number of repetitions was evaluated (Validation Analysis).

Normative modeling for the expressions of leading functional modes

For each leading mode, we charted the normative age-related trajectory of its expression using a normative modeling framework (Fig. 1B). Specifically, we modeled age-related PF variations in the TD population using Gaussian process regression (GPR) [30]. GPR provides a flexible Bayesian framework that captures nonlinear relationships between variables while providing uncertainty estimates [51]. Model performance was evaluated with 10-fold cross-validation, after which the normative model was refitted using the full TD population to obtain predicted PF values and associated variances (Supplement). To reduce potential confounding effects, FSIQ and head motion metrics (i.e., mean FD) were regressed out from PF values prior to normative modeling and subsequent deviation estimation. The regression was performed separately within the TD and ASD groups using a generalized linear model.

Estimating individual deviations based on normative models

For each TD and ASD participant, we estimated individual deviations in the expressions of the K leading modes (i.e., PFs) relative to the normative age-related trajectories by mapping individual PF values onto normative percentile charts (Fig. 1C). Specifically, for each individual, mode-specific deviation scores (Z) were computed by comparing observed PF values with age-predicted PF values derived from the normative model (Supplement) [30].

For each leading mode, group differences in PF deviations between the ASD and TD groups were assessed using two-sample t-tests. The false discovery rate (FDR) method was applied to correct for multiple comparisons across the K modes [52].

To characterize interindividual variability in functional deviation profiles within the ASD group, we computed the standard deviation and interquartile range of PF deviations for each mode. Using PF deviations across the five leading modes as feature vectors, we then computed pairwise Euclidean distances between individuals and compared the resulting distances between the ASD and TD groups using two-sample t-tests. Finally, we examined the distribution of ASD individuals showing extreme deviations across modes. Extreme deviations were defined as $|Z| > 2.6$ for each mode, corresponding to $p < 0.005$ [30].

Identifying ASD subtypes based on individual PF deviations

We applied the k-means clustering algorithm to each individual PF deviation profile across the K leading modes to identify ASD subtypes with distinct functional deviation patterns (Fig. 1C; Supplement). The optimal cluster number was determined using a voting procedure implemented in the NbClust package, which integrates 23 complementary clustering indices [53]. This procedure consistently supported a two-subtype solution (Results). We then compared PF deviations, demographic variables, and clinical characteristics of ADI-R, ADOS-2, and SRS between the two subtypes (Supplement). Both p values and Cohen's d effect sizes were reported [54].

Next, we examined subtype-specific alterations in functional activity and connectivity (Fig. 1D). At the activity level, a principal deviation pattern of functional activity was derived as a weighted combination of the leading modes, with weights defined by the mean PF deviation of each mode across individuals within a subtype (Supplement). At the connectivity level, the principal deviation pattern of functional connectivity was defined as the aggregate of mode-specific coactivation deviations across modes (Supplement).

Brain-symptom association analysis

We conducted canonical correlation analysis (CCA) [55] to examine associations between PF deviations and clinical symptoms, both within each ASD subtype and across the entire ASD group (Fig. 1D). Clinical measures included subscale scores from the ADI-R, ADOS-2, and SRS (Table S3; Supplement). For each leading mode and each symptom scale, CCA was performed between mode-specific PF deviations and the corresponding symptom subscale scores, after regressing out age effects. Statistical significance was evaluated using permutation testing (10,000 permutations), with PF deviations randomly shuffled across individuals. The FDR method was applied to correct for multiple comparisons across leading modes and symptom scales (i.e., 5 modes × 3 scales).

Cortical thickness analysis of ASD subtypes

Motivated by prior evidence of structure-function associations in the human brain [25], we explored whether ASD subtypes differed in brain morphology. Here, we focused on cortical thickness, a macrostructural measure frequently reported to be altered in ASD [39–41]. For each participant, cortical thickness was estimated at the vertex level using the projection-based thickness (PBT) method implemented in CAT12 [56] and spatially smoothed with a 12-mm Gaussian kernel. Vertex-wise thickness estimates were then summarized into 1,000 cortical nodes. ComBat harmonization [46] was further applied to mitigate site-related effects while retaining age and FSIQ as regressors to preserve biologically meaningful variability. Nodal thickness values were subsequently standardized into z scores by subtracting the whole-brain mean and dividing by the standard deviation, to ensure comparability across participants.

After regressing out age and FSIQ, we examined between-group differences in cortical thickness at the nodal, system, and global levels using two-sample t-tests, comparing each ASD subtype with the TD group, as well as directly comparing the two ASD subtypes (Supplement). For the system-level analysis, seven functional systems were defined based on a prior functional network parcellation [50]. The FDR method was used to correct for multiple comparisons at the nodal and system levels, and Bonferroni correction was applied at the global level (i.e., three comparisons). Finally, we identified cortical nodes showing significant cortical thickness alterations shared by both ASD subtypes relative to the TD group.

Functional subtype prediction analysis using altered cortical thickness

We assessed whether altered cortical thickness (ACT) patterns could predict ASD subtype membership at the individual level. For each ASD participant, ACT at node p was defined as [57, 58]:

$$ACT_p = \frac{CT_{\mathrm{ASD},p} - \mathrm{mean}(CT_{\mathrm{TD},p})}{\mathrm{SD}(CT_{\mathrm{TD},p})}. \quad (1)$$

Here, $CT_{\mathrm{ASD},p}$ and $CT_{\mathrm{TD},p}$ denote standardized nodal cortical thickness values for ASD and TD individuals, respectively. $\mathrm{mean}(CT_{\mathrm{TD},p})$ and $\mathrm{SD}(CT_{\mathrm{TD},p})$ denote the mean and the standard deviation of $CT_{\mathrm{TD},p}$ across all TD participants at the same node. Age and FSIQ were regressed out within each clinical group prior to ACT computation. Importantly, the ACT normalization was performed entirely within the structural imaging modality, without incorporating functional information, thereby avoiding information sharing or leakage between structural features and the functional dynamics used for ASD subtyping.

ASD subtype membership was predicted using a random forest classifier with a fully nested 10-fold cross-validation (Fig. 1D, Supplement) [59]. ACT values from 1000 brain nodes served as input features. Within each cross-validation fold, we re-derived the functional subtype labels in both the training and test sets, which served as reference labels for classifier training and prediction assessment, respectively. Specifically, the entire functional subtyping pipeline was exclusively applied in the training set, including nuisance regression of PF values, re-estimation of individual PF deviations, and deviation-based clustering. The resulting nuisance regression models and clustering centers were then applied to the held-out test set, and the re-derived subtype labels were used as reference labels for prediction assessment. For structural features, covariate regression for cortical thickness was conducted solely in the training set and subsequently applied to the test set for ACT computation. Model performance was evaluated using classification accuracy, balanced accuracy, and the area under the receiver operating characteristic curve (AUC) [60], together with the classification confusion matrix. Statistical significance was assessed

using permutation testing (10,000 permutations), with subtype labels randomly shuffled across ASD individuals in the test set. To ensure robustness, the entire procedure was repeated across 100 random train-test splits.

Validation analysis

We assessed the robustness of the main findings through a series of validation analyses, including varying the number of repetitions used to identify leading modes and PFs, applying more stringent head motion criteria, testing alternative regularization and nuisance regression strategies in brain-symptom association analyses, and evaluating imaging site effects (Supplement). In addition, we applied the full pipeline to an independent, out-of-sample dataset (PKUSH) to examine the generalizability of the ABIDE-derived ASD subtypes and their subtype-specific characteristics (Supplement).

RESULTS

Altered deviations in functional state dynamics in ASD individuals

In the TD group, we identified five leading activity modes and their corresponding coactivation patterns using eigen-microstate analysis (Fig. 2A, B). Consistent with previous findings in adults [38], each mode exhibited a distinct topography aligned with prior functional systems (Fig. 2A and Fig. S1). Patterns of interregional coactivation varied across modes (Fig. 2B). Leading mode 1 primarily reflected the antagonistic activity (i.e., anti-coactivation) between the default-mode network and both the somatomotor and ventral attention networks. Mode 2 was characterized by anti-coactivation between the visual and dorsal attention networks and the rest of the brain. Mode 3 reflected anti-coactivation of the dorsal attention and frontoparietal networks with other systems. Mode 4 reflected anti-coactivation of the frontoparietal and ventral networks with other systems. Mode 5 exhibited a more complex pattern, with heterogeneous coactivation within and across functional systems. These results indicate the presence of multiplexed relationships between different networks.

We estimated the expressions (i.e., PF values) in five leading modes for both TD and ASD individuals. For each leading mode, the typical age-related trajectory of PFs obtained from the TD group exhibited nonlinear changes or linear decreases with age (Fig. 2C). The models demonstrated robust fits, as indicated by high explained variance and low standardized log-loss in 10-fold cross-validation (Fig. S2). Compared with TD controls, individuals with ASD showed significantly different deviations in three modes, with opposite-direction PF deviations in mode 2 and greater negative deviations in modes 3 and 4 (all p_{FDR}s < 0.001; Fig. 2D).

Moreover, we observed that individual deviations of PF values were widely dispersed within each mode for the ASD group (SD: 0.91-1.11, IQR: 1.14-1.51; Fig. 3A). Compared with the TD controls, the ASD group exhibited significantly greater distances between deviation profiles of individuals ($p < 0.001$; Fig. 3B), reflecting higher interindividual variability in the ASD group. Furthermore, 49 individuals with ASD exhibited extreme deviations, and most of them (93.9%) showed extreme deviations in only one leading mode, primarily in mode 2 or 3 (Fig. 3C, D), indicating the importance of extracting diverse leading modes.

Identification of ASD subtypes based on PF deviations

Using k-means clustering of individual PF deviation profiles, we identified two ASD subtypes, each comprising 113 and 327 individuals separately. The distribution of subtype membership across sites is shown in Table S4. Both subtypes showed greater positive PF deviations in leading mode 2 and greater negative deviations in leading modes 3 and 4 relative to TD controls (all p_{FDR}s < 0.05; Fig. 4A). Compared with subtype 2 ($n = 327$), subtype 1 ($n = 113$) showed greater positive deviations in leading modes 1 and 2, and milder negative deviations in leading modes 3 and 4 (all p_{FDR}s < 0.05; Fig. 4A, B). Importantly, a greater positive deviation in mode 1 was observed only in subtype 1 relative to TD controls. This difference was not detected in the full ASD group (Fig. 2D), highlighting the value of subtyping to detect ASD-related alterations.

We compared demographic and clinical characteristics between two subtypes. Compared with subtype 2, individuals with subtype 1 showed greater mean FD ($p = 0.002$) and higher scores for restricted and repetitive behaviors, social cognition, communication, and mannerisms but lower scores for social affect and calibrated severity (all ps < 0.05, absolute Cohen's d values > 0.3; Table 2).

We further assessed the functional dysfunctions in terms of functional activity and connectivity. Relative to the age-expected normative pattern, subtype 1 showed increased activity amplitudes primarily in the default-mode and frontoparietal networks and decreased amplitudes in the dorsal attention and visual networks. Subtype 2 showed increased amplitudes primarily in the frontoparietal and ventral attention networks and decreased amplitudes in the somatomotor and visual networks (Fig. 4C).

The connectivity patterns also differed between subtypes (Fig. 4D). Relative to the age-expected normative pattern, subtype 1 showed increased FC primarily within the visual, default-mode, and ventral attention networks, as well as between the visual and dorsal attention networks and between the somatomotor and ventral attention networks. In contrast, decreased FC was mainly observed between the visual network and both the default-mode and ventral attention networks. Subtype 2 exhibited increased FC primarily between the somatomotor and frontoparietal networks and between the visual and dorsal attention networks, whereas decreased connectivity was primarily found within the somatomotor, dorsal attention, and frontoparietal networks.

Associations between individual functional deviations and clinical symptoms

For each leading mode, we performed CCA between PF deviations and combined symptom subscales within each ASD subtype and the full ASD group. PF deviations in leading modes 4 and 5 were significantly correlated with SRS scores in both subtypes (all rs ≥ 0.28, p_{FDR}s < 0.05; Fig. 5A, B). However, the relative contributions of symptom subscales varied between subtypes, particularly in the domains of social cognition, communication, motivation, and autistic mannerisms.

Subtype-specific associations were also observed. In subtype 1, PF deviations on leading mode 2 were correlated with ADI-R scores ($r = 0.27$, $p_{FDR} = 0.0439$), driven primarily by positive weights in the verbal domain, and with SRS scores ($r = 0.36$, $p_{FDR} = 0.0259$), dominated by positive weights in social awareness and negative weights in social motivation (Fig. 5A). In subtype 2, PF deviations in leading mode 3 were correlated with SRS scores ($r = 0.31$, $p_{FDR} = 0.0093$), mainly driven by negative weights in social cognition, communication, motivation, and autistic mannerisms (Fig. 5B). In contrast, only one significant association was observed in the full ASD group, which was between PF deviations in mode 4 and SRS scores ($r = 0.24$, $p_{FDR} = 0.0267$; Fig. S3). No significant associations were found with ADOS-2 scores, regardless of the leading mode or subtype (all p_{FDR}s > 0.05).

Altered cortical thickness in ASD subtypes

Compared with TD controls, both ASD subtypes exhibited significantly greater global cortical thickness (all ps < 0.001, Bonferroni corrected; Fig. 6A). At the node level, widespread alterations were observed in 82.6% and 82.0% of the brain nodes for subtypes 1 and 2, respectively (all p_{FDR}s < 0.05, Fig. 6B), with 67.6% of the altered nodes overlapping between subtypes (Fig. S4). Additionally, 82.2% of the brain nodes showed significant

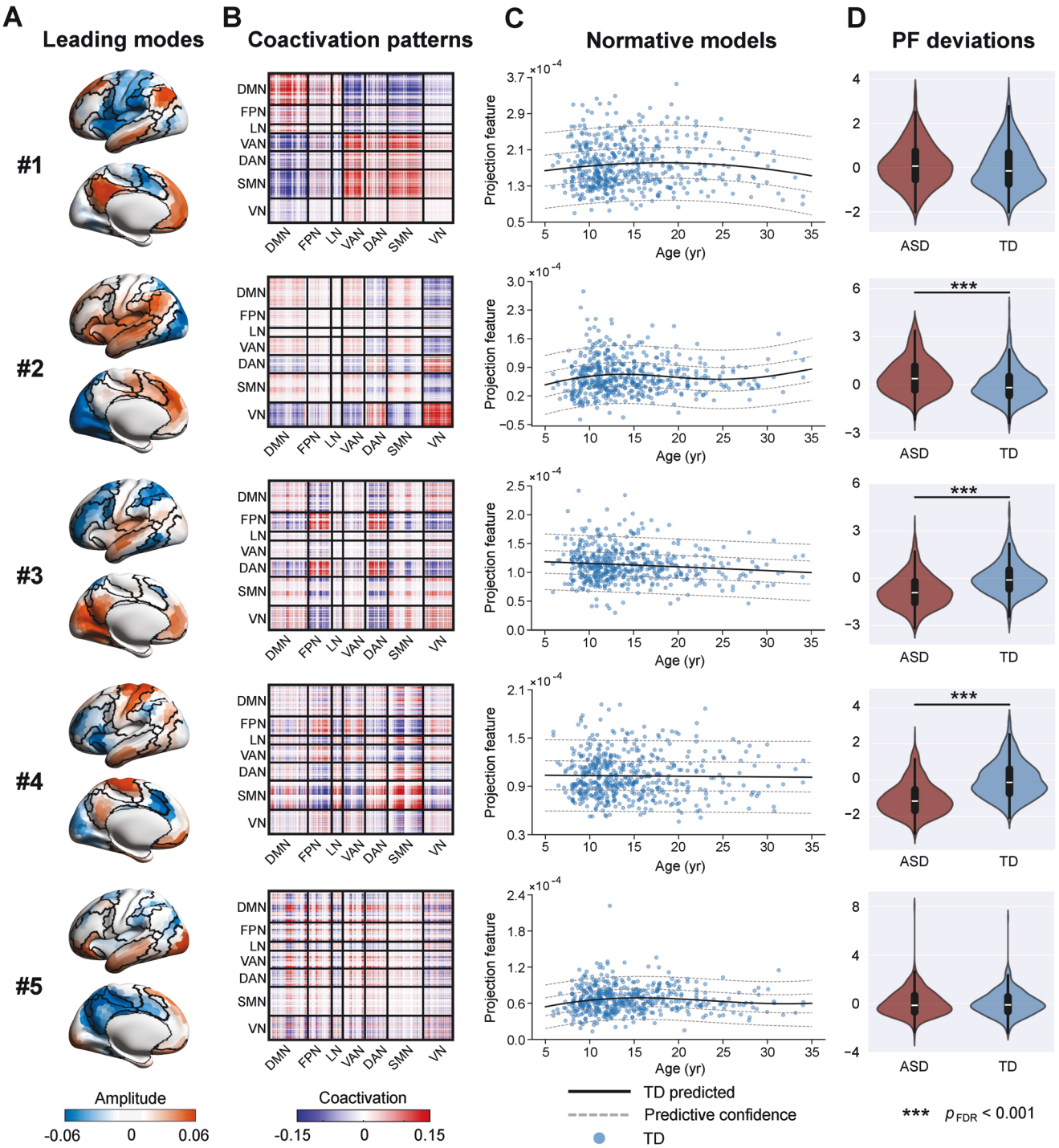

Fig. 2 Identification of individual deviations in leading mode expressions and corresponding between-group differences. A Spatial maps of five leading modes in the typically developing group, derived via eigen-microstate analysis (left hemisphere shown). Black contours delineate seven functional systems defined in a prior brain template [50]. **B** Nodal-level coactivation pattern for each leading mode, with black lines marking seven functional systems. **C** Normative age-related trajectories of projection features (PFs) for the five leading modes, estimated using Gaussian process regression. Blue dots represent PFs of typically developing participants. The solid line denotes the median (50th percentile), and dashed lines indicate the 5th, 25th, 75th, and 95th percentiles. The small numerical scale (10^{-4}) of PFs arose from normalization of the time courses prior to singular value decomposition (SVD), which reduced the activity amplitude. **D** Between-group comparisons of PF deviations in each leading mode between the autism spectrum disorder and the typically developing groups (two-sample t-tests). ASD autism spectrum disorder, TD typically developing, DMN default-mode network, FPN frontoparietal network, LN limbic network, VAN ventral attention network, DAN dorsal attention network, SMN somatomotor network, VN visual network, yr year, p_{FDR} false discovery rate-corrected *p*-value.

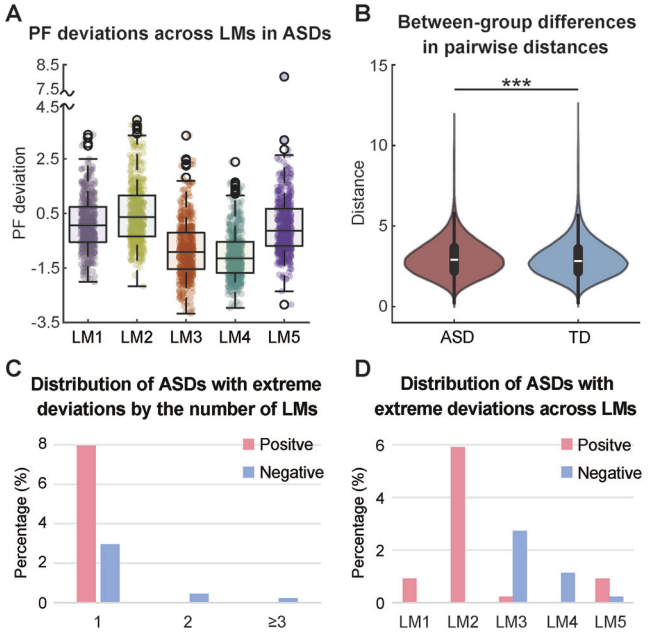

Fig. 3 Individual difference in functional deviations for participants with autism spectrum disorder (ASD). A Individual deviations in leading mode expressions for participants with ASD. **B** Comparisons of interindividual distances in functional deviation profiles between ASD and typical developing groups (two-sample t-tests). Interindividual pairwise distances were calculated using the Euclidean metric. **C** Distribution of ASD individuals by the number of leading modes exhibiting extreme positive (red) or negative (blue) deviations. **D** Numbers of ASD individuals exhibiting extreme positive (red) or negative (blue) deviations in each mode. TD typically developing, LM leading mode, PF projection feature.

differences in cortical thickness between the two subtypes (all p_{FDR}s < 0.05, Fig. 6B).

At the system level, both ASD subtypes showed greater thickness in the ventral attention and somatomotor networks and decreased thickness in the frontoparietal, dorsal attention, and limbic networks compared with TD controls (all p_{FDR}s < 0.05). However, the two subtypes diverged in the default-mode and visual networks: subtype 1 showed greater thickness in the default-mode network and decreased thickness in the visual network (all p_{FDR}s < 0.05), whereas subtype 2 exhibited the opposite pattern in the default-mode network (p_{FDR} < 0.05) and no significant change in the visual network (p_{FDR} > 0.05). Direct comparisons between subtypes revealed significant differences across all seven functional networks (all p_{FDR}s < 0.05). Opposite alteration patterns were observed in the visual and somatomotor networks relative to the default-mode, limbic, frontoparietal, and attention networks (Fig. 6B).

Using ACT values from 1000 brain nodes as input features, the structural classifier achieved high accuracy in predicting ASD subtype membership (accuracy = 0.83 ± 0.02, balanced accuracy = 0.78 ± 0.02, AUC = 0.84 ± 0.01, all *p*s < 0.001; 100 repetitions, Fig. 6C). The confusion matrix revealed a moderate sensitivity for subtype 1 (66% ± 4%) and high specificity (89% ± 1%) for subtype 2 (Fig. S5). The most discriminative features were primarily located in the medial prefrontal cortex, fusiform gyrus, visual cortex, and somatosensory cortex (Fig. 6D), with relatively low variability across repetitions (Fig. S5). These regions closely overlapped with those showing significant cortical thickness differences between the two subtypes.

Validation results

Overall, the main findings are robust across multiple analysis strategies. The leading modes and the projection features stabilized after 100 repetitions (Fig. S6). Functional subtypes and subtype-specific functional alterations remained highly consistent under different head motion correction strategies (Figs. S7-S10). Brain-symptom associations were largely preserved across alternative CCA specifications (Figs. S11-S12). Under the leave-one-site-out strategy, ASD subtyping was highly reproducible (Table S5), and subtype prediction achieved an accuracy of 84% when each site was used as an independent test set (Fig. S13). Finally, two functional subtypes of ASD were identified in the independent PKUSH dataset, showing similar functional alterations (Fig. S14) and clinical symptom differences (Table S6). The ABIDE-trained structure-to-subtyping classifier achieved good performance when applied to PKUSH (accuracy = 0.79, balanced accuracy = 0.74, AUC = 0.78; Fig. S14). The relatively lower accuracy compared with ABIDE may be due to the smaller ASD size in PKUSH and population differences.

DISCUSSION

This study demonstrates profound interindividual heterogeneity in the functional state dynamics of spontaneous brain activity in ASD. Using normative modeling, we quantified individual deviations in the expressions of five leading activity modes and identified two reproducible ASD subtypes across imaging sites in the ABIDE dataset. These subtypes exhibited divergent, mode-specific alterations in functional activity and connectivity and were clinically dissociable with distinct brain-symptom associations. Moreover, they showed different cortical thickness alterations, and subtype membership could be predicted at the individual level from altered cortical thickness patterns. The major findings were replicated in an independent, out-of-sample dataset. Together, these results underscore substantial heterogeneity in connectome dynamics and its potential anatomical substrates in ASD, providing new insights into the neurobiological mechanisms underlying ASD heterogeneity.

ASD-related heterogeneity and abnormal deviations in functional state dynamics

In this study, we investigated heterogeneity in whole-brain functional state dynamics in ASD beyond traditional case-control comparisons [11–13]. We focused on individual deviations in the functional state expressions (i.e., leading mode expressions), while accounting for age-related effects using normative modeling [30–33]. Consistent with prior studies [38, 61], we identified a small set of representative functional states, supporting the reproducibility of this low-dimensional organization of spontaneous activity across populations. These leading modes exhibited system-dependent spatial patterns and have been linked with distinct cognitive profiles [38], suggesting that they capture biologically meaningful axes of brain organization. Notably, the eigen-microstate analysis represents each moment as a weighted combination of leading modes, capturing continuous and overlapping dynamics. This state definition differs from sliding-window or dynamic independent component analysis approaches, which typically assign each time window to a single brain state [14]. Consistent with our findings, altered overlapping brain state dynamics has also been observed in other psychiatric disorders using nonlinear manifold learning [62]. These complementary frameworks underscore the value of functional state dynamics for probing the neural mechanisms underlying brain disorders.

Individuals with ASD exhibited mode-dependent, aberrant deviations in leading mode expressions (i.e., PFs), with prominent effects in modes 2-4. At the individual level, deviation profiles are highly heterogeneous. Extreme deviations were largely restricted to a single mode (mostly modes 2, 3, and 4) and showed low cross-individual consistency (< 6%). This observation suggests multiplexed coordination among brain regions and highlights the fine-grained, individualized nature of connectome dynamics

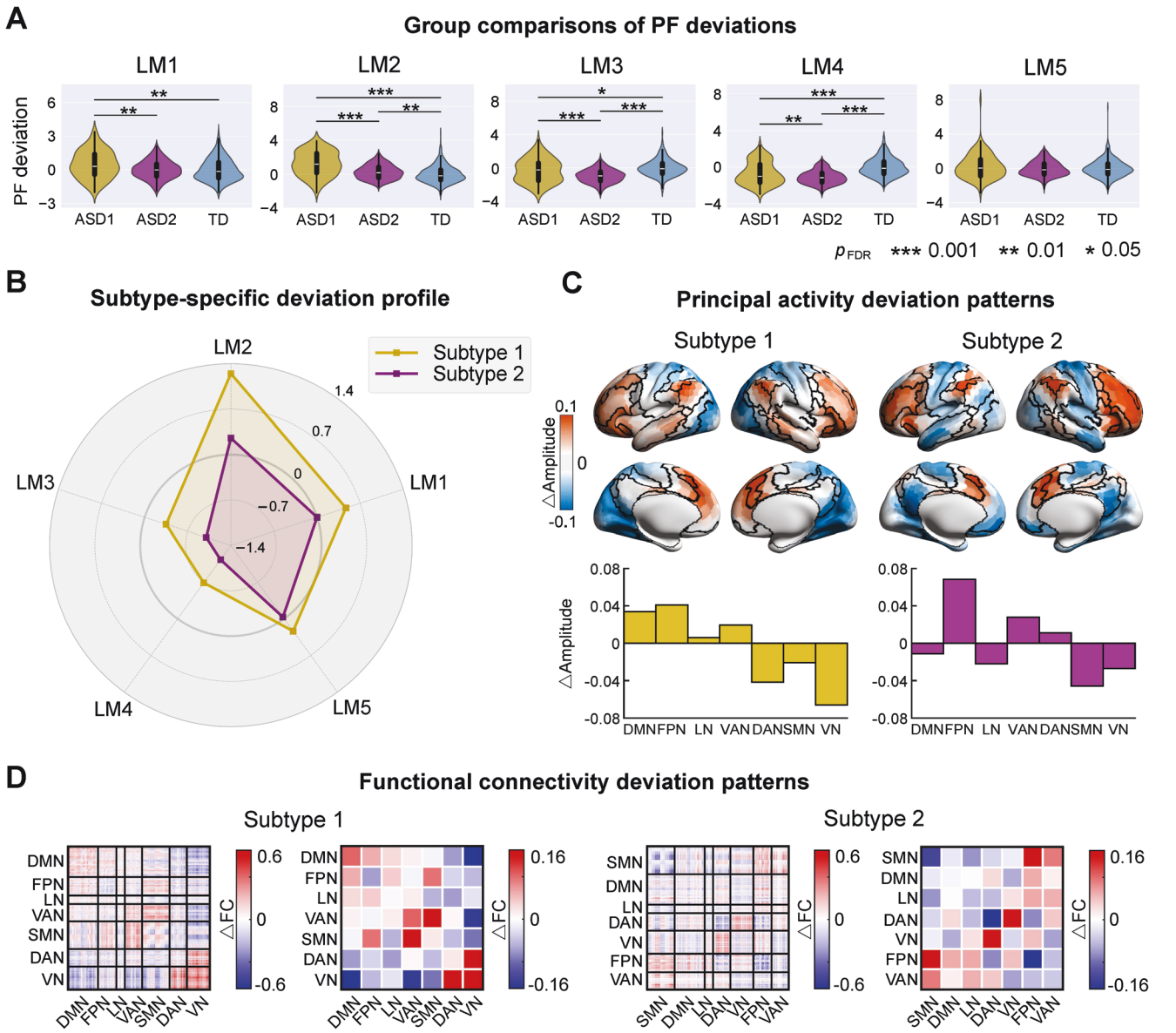

Fig. 4 Subtype-specific deviations in projection features (PFs) and functional organization. A PF deviations in each leading mode were compared between each autism spectrum disorder (ASD) subtype and the typically developing group, as well as between the two ASD subtypes (two-sample t-tests). **B** Mean PF deviations across five leading modes within each ASD subtype (i.e., cluster centers). **C** Principal deviation patterns of functional activity for each subtype. Deviations in subtype 1 primarily involved the visual, default-mode, frontoparietal, and dorsal attention networks. Deviations in subtype 2 primarily involved the somatomotor, visual, frontoparietal, and ventral attention networks. Brain maps show nodal-level patterns, and bar plots summarize system-level patterns. **D** Functional connectivity deviation patterns at the nodal and system levels for each subtype. TD typically developing, LM leading mode, ASD1 ASD subtype 1, ASD2 ASD subtype 2, p_{FDR} false discovery rate-corrected *p*-value, ΔAmplitude activity amplitude deviations, ΔFC functional connectivity deviations, DMN, default-mode network, FPN frontoparietal network, LN limbic network, VAN ventral attention network, DAN dorsal attention network, SMN somatomotor network, VN visual network.

alterations in ASD. These three modes were characterized by coordinated activity between visual and somatomotor networks and other high-order networks, including the default-mode, frontoparietal, and attention networks. Such configurations are consistent with established functional hierarchies supporting sensory processing, self-referential processing, and executive control [38, 63]. In contrast, mode 1 showed fewer extreme deviations at the individual level, suggesting the relative stability of individual deviations in this mode. Spatially, this mode reflects the separation between primary and association cortices [63, 64], which may be tightly constrained by basic neurophysiological processes. Prior work has reported its role as a shared and fundamental functional component across individuals [38, 65], and it tends to remain relatively stable despite disease-related alterations. Together, these findings reveal mode-specific patterns of functional deviations in ASD, which are not present in static connectivity measures. These heterogeneous functional deviations may relate to individual-specific age-related changes during neurodevelopment [66]. By integrating low-dimensional dynamic features with normative modeling, our study provides a novel approach to characterize individualized disruptions of brain dynamics in ASD. This approach extends beyond traditional static or temporally averaged measures of functional connectivity [3, 4, 8, 24].

Table 2. Demographic and clinical characteristics of two ASD subtypes in the ABIDE cohort.

	Subtype 1 ($n = 113$)	Subtype 2 ($n = 327$)	Cohen's d	p Value
Age, years	14.72 ± 5.33 (113)	14.13 ± 5.40 (327)	0.111	0.309
FSIQ	106.77 ± 16.38 (113)	107.18 ± 16.71 (327)	-0.025	0.822
Mean FD, mm	0.23 ± 0.11 (113)	0.19 ± 0.09 (327)	0.348	0.002**
ADI-R				
Social	18.24 ± 4.76 (85)	18.44 ± 5.44 (270)	-0.036	0.772
Verbal	15.43 ± 4.17 (85)	15.18 ± 4.53 (271)	0.058	0.644
RRB	6.22 ± 2.15 (85)	5.45 ± 2.60 (271)	0.308	0.007**
Onset	3.36 ± 1.39 (85)	3.20 ± 1.33 (232)	0.117	0.356
ADOS-2				
Total	9.28 ± 3.92 (60)	10.44 ± 4.57 (197)	-0.260	0.079
Social affect	5.54 ± 3.63 (60)	7.98 ± 3.77 (194)	-0.650	<0.001***
RRB	3.60 ± 1.51 (62)	2.64 ± 1.74 (195)	0.566	<0.001***
Severity	5.70 ± 1.91 (60)	6.46 ± 2.05 (197)	-0.376	0.011*
SRS				
Total	102.02 ± 24.56 (85)	83.85 ± 31.04 (204)	0.618	<0.001***
Awareness	13.66 ± 3.10 (60)	12.75 ± 4.18 (108)	0.237	0.113
Cognition	18.30 ± 5.32 (60)	13.83 ± 6.30 (108)	0.746	<0.001***
Communication	36.98 ± 8.95 (60)	28.37 ± 11.25 (108)	0.816	<0.001***
Motivation	13.82 ± 5.80 (60)	12.01 ± 6.22 (108)	0.297	0.067
Mannerisms	21.52 ± 6.37 (60)	14.63 ± 7.32 (108)	0.979	<0.001***

All values are presented as mean ± SD (participant number available).
All p values were obtained from two-sample t-tests; *$p < 0.05$; **$p < 0.01$; ***$p < 0.001$. For each clinical measure, we considered participants with the corresponding scores available.
ASD autism spectrum disorder, *FSIQ* full-scale intelligence quotient, *Mean FD* mean framewise displacement, *ADI-R* autism diagnostic interview-revised, *RRB* restricted and repetitive behavior, *ADOS-2* autism diagnostic observation schedule-second edition, *SRS* social responsiveness scale.

ASD subtypes based on functional state dynamics deviations

To further delineate individual differences, we identified two ASD subtypes showing distinct deviation profiles across the first four leading modes. These two subtypes are reproducible across imaging sites in the ABIDE and replicated in an out-of-sample dataset. Compared with the TD group, subtype 1 displayed additional deviations in mode 1, which was absent in the full ASD group. These findings highlight the importance of accounting for within-group heterogeneity. Both subtypes shared alterations in the visual and frontoparietal networks. The ASD-related functional alterations in these networks have been linked with sensory hypersensitivity [67, 68] and reduced cognitive control [69]. Beyond these shared disruptions, these two subtypes diverged in additional network alterations, indicating divergent sensory and cognitive processing abnormalities. Subtype 1 exhibited extra dysfunctions in the default-mode and dorsal attention networks, potentially related to ASD-related excessive internally directed thought [70] and impaired interpretation of visual social cues [67, 68]. Subtype 2 showed additional alterations in the somatomotor and ventral attention networks, which may underlie motor and imitation deficits [71] and attentional impairments in ASD [72]. Interestingly, these functional distinctions mirror prior subtyping based on static FC, which reported one subtype with hyperconnectivity in the default-mode/salience networks and another with somatomotor network disruptions [73]. The divergent network alterations may contribute to clinical differences between subtypes. Subtype 1 exhibited more severe restrictive and repetitive behaviors and greater social responsiveness impairments than subtype 2, with medium to large effect sizes, indicating that the subtypes are clinically distinguishable. Notably, head motion differed between subtypes despite stringent correction, suggesting that it may reflect neurobiologically relevant traits rather than mere measurement noise [74–76]. This finding highlights the careful consideration of motion in future ASD studies.

The associations between functional dynamics deviations and clinical symptoms were both mode-dependent and subtype-specific, which are not driven by specific site bias. This pattern suggests that distinct neurophysiological mechanisms may underlie phenotypic heterogeneity in ASD. In both subtypes, deviations in leading modes 4 and 5 correlated with social motivation deficits and stereotyped behaviors. These two modes are linked to higher-order cognitive functions, including inhibitory control, motor regulation, working memory, reward processing, and language expression [38]. Their disruptions may represent shared substates of core ASD symptoms. Subtype-specific patterns also emerged. In subtype 1, deviations in mode 2 were associated with impairments in social communication and awareness. Mode 2 coordinates activity across visual, default-mode, and salience networks. Its disruptions may impair the integration of perceptual input with self-referential and salience processing [67, 68, 70], reducing the capacity to extract and prioritize socially relevant cues. In subtype 2, deviations in mode 3 were associated with broad impairments in social responsiveness. Mode 3 reflects interactions within and between frontoparietal and dorsal attention networks, which are essential for recognizing emotions and intentions [71] and adapting to dynamic social cues [69]. Collectively, these findings indicate that subtype-specific disruptions in functional state dynamics are linked to distinct clinical profiles, highlighting their potential as clinically informative markers for stratification and individualized interventions in ASD.

Distinct structural substrates of two functional subtypes

Previous studies have reported widespread cortical thickness abnormalities in ASD [40], particularly in the prefrontal, parietal, and temporal cortices [39–41, 77–79]. These alterations also

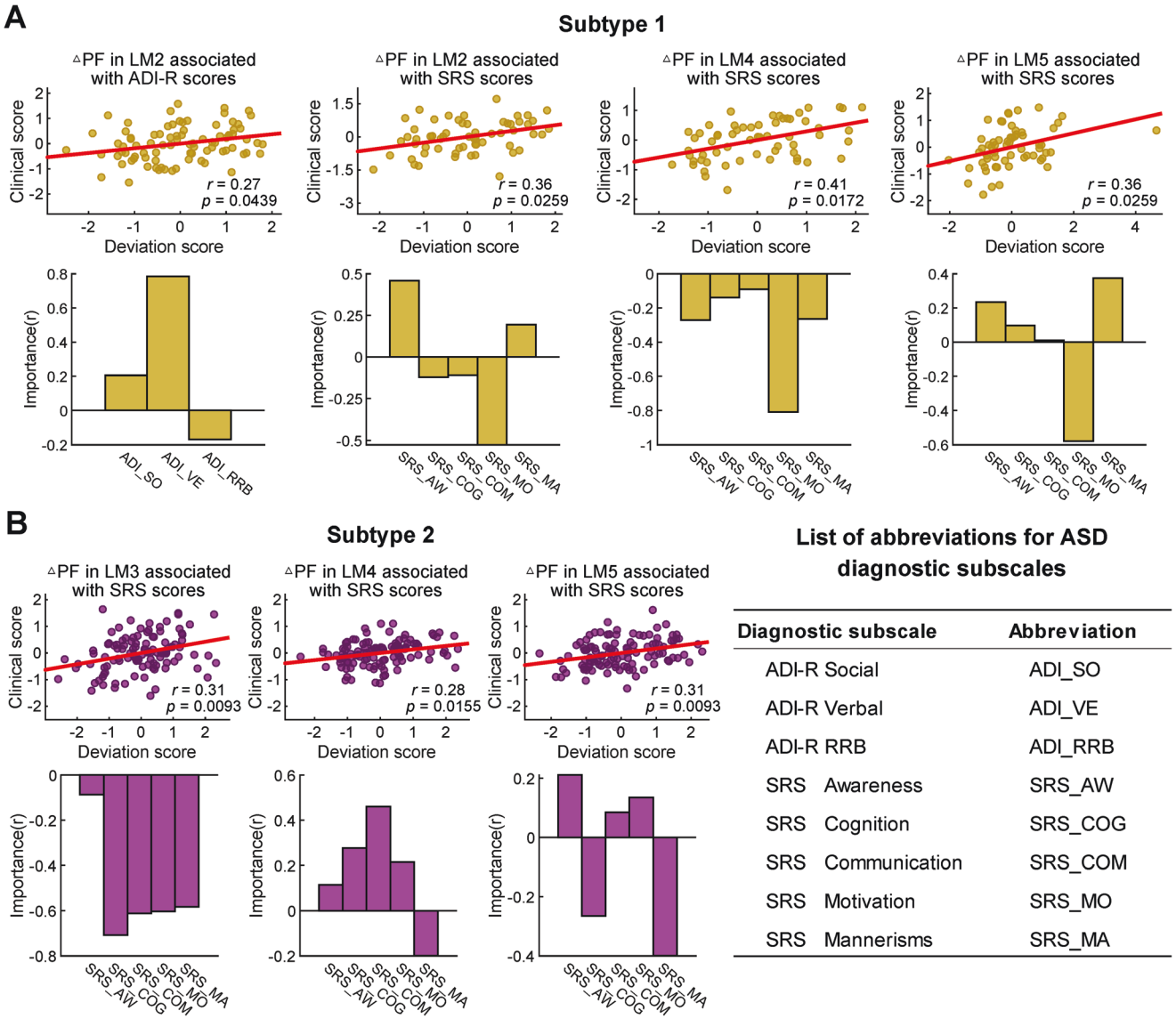

Fig. 5 Association patterns between projection feature (PF) deviations and clinical symptoms in two subtypes. A Association in Subtype 1. **B** Association in Subtype 2. Canonical correlation analyses were conducted between PF deviations in each leading mode and aggregated clinical subscale scores derived from three diagnostic instruments (see Supplement). Each scatter plot shows a significant association between the canonical PF deviation score and the canonical clinical score, with each dot representing an individual with autism spectrum disorder. All *p*-values displayed were corrected with the false discovery rate method across leading modes and symptom scales (i.e., 5 modes × 3 scales). Bar plots display the canonical loadings, defined as Pearson's correlation between individual subscales and the corresponding canonical clinical score. The table lists the full names and abbreviations of clinical subscales displayed in the bar plots. ASD autism spectrum disorder, ΔPF projection feature deviations, LM leading mode, RRB restricted and repetitive behavior, ADI-R Autism Diagnostic Interview-Revised, SRS Social Responsiveness Scale.

exhibit considerable interindividual variability in both spatial distribution and direction of change [32, 41]. Consistent with these findings, both functional subtypes identified here exhibited distributed cortical thickness alterations. Shared patterns across subtypes predominantly involved the somatomotor, frontoparietal, ventral/dorsal attention, and limbic networks, reflecting common structural disruptions in ASD. Notably, these two subtypes diverged in cortical thickness within the default-mode and visual networks, paralleling their distinct functional deviation profiles. In contrast, other networks, such as the frontoparietal and somatomotor networks, showed discordant structural and functional alterations, suggesting complex, region-specific coupling. These subtype-specific alterations may correspond to distinct neurocognitive phenotypes, with subtype 1 associated with heightened internally directed processes and subtype 2 with increased perceptual sensitivity. These clinical differences have been frequently observed in ASD [57, 80].

Importantly, ASD subtype membership, defined by functional dynamics deviations, could be predicted with high accuracy from cortical thickness alterations. This finding was replicated in multiple validation analyses, including an independent PKUSH dataset, underscoring the role of anatomical substrates in shaping functional dynamics. Notably, while subtype 2 membership was reliably identified, a proportion of subtype 1 individuals were misclassified, likely reflecting the inherent heterogeneity in functional features within subtype 1. Prior work has shown that cortical thickness undergoes coordinated thinning during childhood and adolescence, in parallel with developmental changes in FC patterns [81]. Thus, the atypical development of cortical thickness may contribute to altered functional dynamics in ASD.

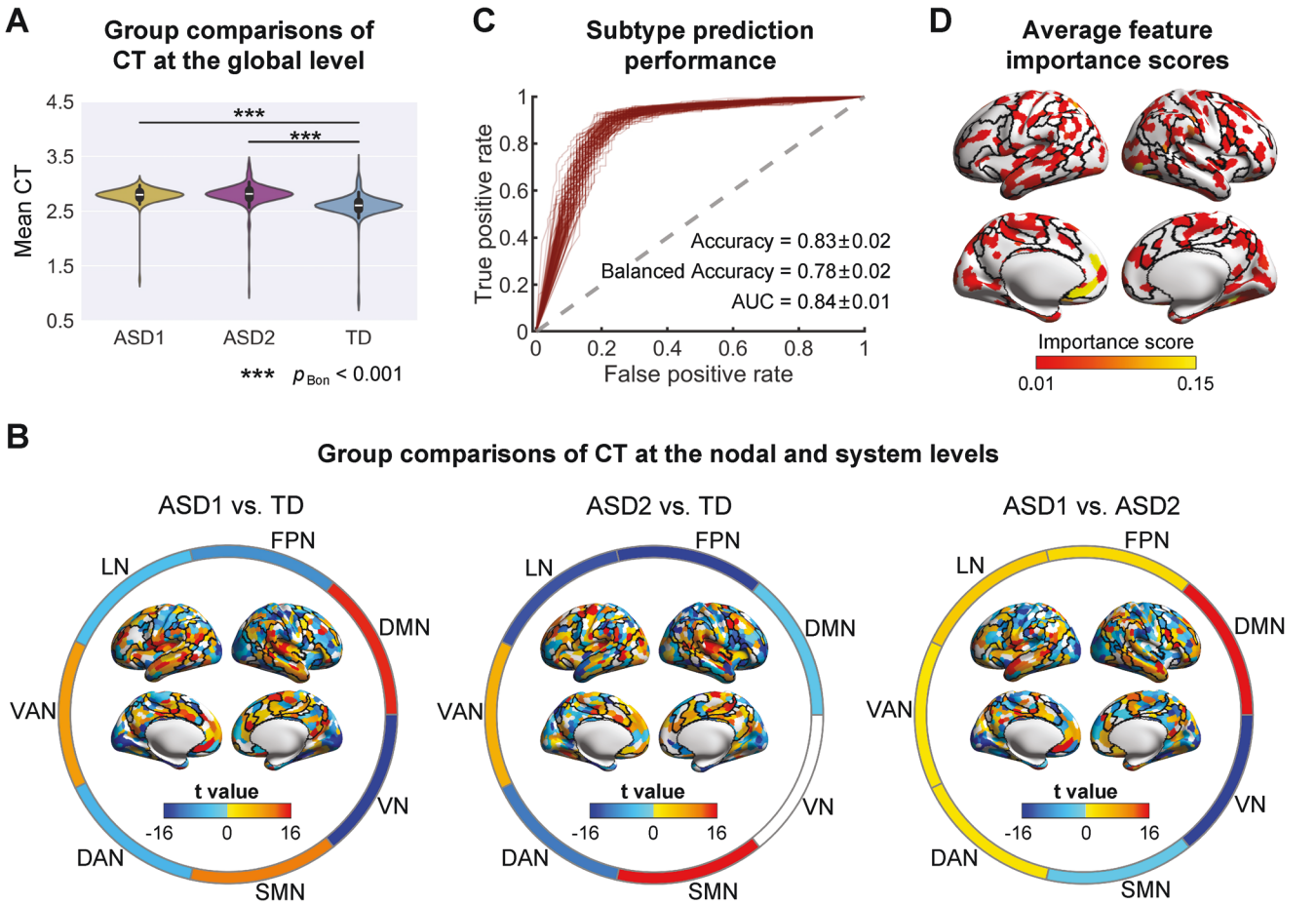

Fig. 6 Subtype-specific structural characteristics in cortical thickness. A Comparison of global cortical thickness among autism spectrum disorder (ASD) subtype 1, subtype 2, and typically developing controls. **B** Group differences in cortical thickness at the nodal and system levels among ASD subtypes and the typically developing group (two-sample t-tests, all *ps* < 0.05, false discovery rate corrected). Nodal-level *t*-values are shown on brain maps, and system-level *t*-values are presented as circular plots. **C** Subtype prediction using a random forest classification model. Red curves represent receiver operating characteristic (ROC) curves from each of 100 random splits of the training and test sets, and the gray dashed line indicates chance-level performance. True positive rate, samples with original subtype 1 correctly predicted as subtype 1; False positive rate, samples with original subtype 2 incorrectly predicted as subtype 1. **D** Nodal contribution to the subtype prediction. The brain map shows the average feature importance scores across 100 splits for each brain node. TD typically developing, ASD1 ASD subtype 1, ASD2 ASD subtype 2, CT cortical thickness, DMN default-mode network, FPN frontoparietal network, LN limbic network, VAN ventral attention network, DAN dorsal attention network, SMN somatomotor network, VN visual network, p_{Bon} Bonferroni-corrected *p*-value, AUC area under the ROC curve.

Cortical thinning reflects microstructural changes, including synaptic pruning [82] and intracortical myelination [83]. Integrating local morphological features into computational dynamic models may help clarify how structural abnormalities give rise to altered functional dynamics [84, 85]. Such efforts would advance our understanding of the anatomical basis of functional heterogeneity in ASD.

Conclusions and future work

Our study reveals substantial interindividual variability in functional state dynamics in ASD, identifies neurophysiologically and clinically distinct ASD subtypes, and links this heterogeneity in connectome dynamics to underlying structural morphology. These findings offer novel insights into the neural mechanisms underlying ASD heterogeneity and introduce an individualized, clinically sensitive framework for subtyping, with potential implications for ASD and other psychiatric conditions.

Several issues warrant further consideration. First, the current sample included only male participants, due to the higher prevalence of ASD in males and the limited number of female participants in ABIDE. Prior studies have reported sex-specific alterations in static functional organization [86–88] and connectome dynamics [89]. However, functional subtyping studies that included females have not reported within-subtype sex effects [24, 73, 90]. Thus, it remains unclear whether the functional subtypes identified here would generalize to female samples, underscoring the need for further investigation with adequately powered female cohorts. Second, age-related trajectories of PFs were estimated from cross-sectional data, which may be influenced by individual differences unrelated to development. In the future, incorporating longitudinal data would allow a more precise characterization of developmental changes within the normative modeling framework [91, 92]. Third, discrepancies were observed between caregiver-reported and clinician-assessed symptom measures, with subtype 1 showing greater restricted and repetitive behaviors and social difficulties despite showing lower clinician-rated severity. This likely reflects informant discordance in the assessment of social skills [93, 94] and underscores the need for multi-informant phenotyping [95]. Finally, information on psychiatric comorbidities and medication status was not available for participants used here. These factors

are known to influence functional organization and symptom measures [96–98], and may therefore affect functional subtyping and brain-symptom associations. They may also contribute to the discrepancies between caregiver-reported and clinician assessments mentioned above. Future studies incorporating detailed comorbidity, treatment information, or other clinical populations will help clarify which functional alterations are ASD-specific or shared with other conditions.

DATA AVAILABILITY

The ABIDE datasets are publicly available (https://fcon_1000.projects.nitrc.org/indi/abide/). The PKUSH dataset is available from the corresponding author (L.Y.) upon reasonable request. The Schaefer-1000 cortical atlas was used for brain parcellation definition (https://github.com/ThomasYeoLab/CBIG/tree/master/stable_projects/brain_parcellation/Schaefer2018_LocalGlobal).

CODE AVAILABILITY

All software packages used in this study are publicly available, including GRETNA (http://www.nitrc.org/projects/gretna/), CAT12 (https://neuro-jena.github.io/cat/), ComBat harmonization (https://github.com/Jfortin1/ComBatHarmonization), Normative modelling via PCNtoolkit (https://github.com/amarquand/PCNtoolkit), NbClust (https://www.rdocumentation.org/packages/NbClust/versions/3.0.1/topics/NbClust), and mvlearn (https://github.com/mvlearn/mvlearn). All custom codes used in this work are available from the corresponding author (X.H.L.) upon reasonable request.

REFERENCES

1. Lord C, Brugha TS, Charman T, Cusack J, Dumas G, Frazier T, et al. Autism spectrum disorder. Nat Rev Dis Primers. 2020;6:5.
2. Lai M-C, Lombardo MV, Baron-Cohen S. Autism. Lancet. 2014;383:896–910.
3. Li X, Zhang K, He X, Zhou J, Jin C, Shen L, et al. Structural, functional, and molecular imaging of autism spectrum disorder. Neurosci Bull. 2021;37:1051–71.
4. Guo Z, Tang X, Xiao S, Yan H, Sun S, Yang Z, et al. Systematic review and meta-analysis: multimodal functional and anatomical neural alterations in autism spectrum disorder. Mol Autism. 2024;15:16.
5. Hutchison RM, Womelsdorf T, Allen EA, Bandettini PA, Calhoun VD, Corbetta M, et al. Dynamic functional connectivity: promise, issues, and interpretations. Neuroimage. 2013;80:360–78.
6. Liao X, Cao M, Xia M, He Y. Individual differences and time-varying features of modular brain architecture. Neuroimage. 2017;152:94–107.
7. Zalesky A, Fornito A, Cocchi L, Gollo LL, Breakspear M. Time-resolved resting-state brain networks. Proc Natl Acad Sci USA. 2014;111:10341–6.
8. Falahpour M, Thompson WK, Abbott AE, Jahedi A, Mulvey ME, Datko M, et al. Underconnected, but not broken? dynamic functional connectivity MRI shows underconnectivity in autism is linked to increased intra-individual variability across time. Brain Connect. 2016;6:403–14.
9. Zhang J, Cheng W, Liu Z, Zhang K, Lei X, Yao Y, et al. Neural, electrophysiological and anatomical basis of brain-network variability and its characteristic changes in mental disorders. Brain. 2016;139:2307–21.
10. Xie Y, Xu Z, Xia M, Liu J, Shou X, Cui Z, et al. Alterations in connectome dynamics in autism spectrum disorder: a harmonized mega- and meta-analysis study using the autism brain imaging data exchange dataset. Biol Psychiatry. 2022;91:945–55.
11. de Lacy N, Doherty D, King BH, Rachakonda S, Calhoun VD. Disruption to control network function correlates with altered dynamic connectivity in the wider autism spectrum. Neuroimage Clin. 2017;15:513–24.
12. Watanabe T, Rees G. Brain network dynamics in high-functioning individuals with autism. Nat Commun. 2017;8:16048.
13. Fu Z, Tu Y, Di X, Du Y, Sui J, Biswal BB, et al. Transient increased thalamic-sensory connectivity and decreased whole-brain dynamism in autism. Neuroimage. 2019;190:191–204.
14. Calhoun VD, Miller R, Pearlson G, Adalı T. The chronnectome: time-varying connectivity networks as the next frontier in fMRI data discovery. Neuron. 2014;84:262–74.
15. Preti MG, Bolton TAW, Van De Ville D. The dynamic functional connectome: state-of-the-art and perspectives. Neuroimage. 2017;160:41–54.
16. Waterhouse L. Heterogeneity thwarts autism explanatory power: a proposal for endophenotypes. Front Psychiatry. 2022;13:947653.
17. Kuo SS, van der Merwe C, Fu JM, Carey CE, Talkowski ME, Bishop SL, et al. Developmental variability in autism across 17000 autistic individuals and 4000 siblings without an autism diagnosis: comparisons by cohort, intellectual disability, genetic etiology, and age at diagnosis. JAMA Pediatr. 2022;176:915–23.
18. Mottron L. A radical change in our autism research strategy is needed: back to prototypes. Autism Res. 2021;14:2213–20.
19. Lombardo MV, Lai M-C, Baron-Cohen S. Big data approaches to decomposing heterogeneity across the autism spectrum. Mol Psychiatry. 2019;24:1435–50.
20. Mottron L, Bzdok D. Autism spectrum heterogeneity: fact or artifact? Mol Psychiatry. 2020;25:3178–85.
21. Hong S-J, Vogelstein JT, Gozzi A, Bernhardt BC, Yeo BTT, Milham MP, et al. Toward neurosubtypes in autism. Biol Psychiatry. 2020;88:111–28.
22. Guo X, Zhai G, Liu J, Zhang X, Zhang T, Cui D, et al. Heterogeneity of dynamic synergetic configurations of salience network in children with autism spectrum disorder. Autism Res. 2023;16:2275–90.
23. Guo X, Zhang X, Liu J, Zhai G, Zhang T, Zhou R, et al. Resolving heterogeneity in dynamics of synchronization stability within the salience network in autism spectrum disorder. Prog Neuro-Psychopharmacol Biol Psychiatry. 2024;131:110956.
24. Liu Q, Lai H, Le J, Lan C, Zhang X, Huang L, et al. Identifying brain functional subtypes and corresponding task performance profiles in autism spectrum disorder. Mol Psychiatry. 2025;30:5034–44.
25. Suárez LE, Markello RD, Betzel RF, Misic B. Linking structure and function in macroscale brain networks. Trends Cogn Sci. 2020;24:302–15.
26. Liao X, Yuan L, Zhao T, Dai Z, Shu N, Xia M, et al. Spontaneous functional network dynamics and associated structural substrates in the human brain. Front Hum Neurosci. 2015;9:478.
27. Shen K, Hutchison RM, Bezgin G, Everling S, McIntosh AR. Network structure shapes spontaneous functional connectivity dynamics. J Neurosci. 2015;35:5579.
28. Liu J, Xia M, Wang X, Liao X, He Y. The spatial organization of the chronnectome associates with cortical hierarchy and transcriptional profiles in the human brain. Neuroimage. 2020;222:117296.
29. Sun L, Liang X, Duan D, Liu J, Chen Y, Wang X, et al. Structural insight into the individual variability architecture of the functional brain connectome. Neuroimage. 2022;259:119387.
30. Marquand AF, Rezek I, Buitelaar J, Beckmann CF. Understanding heterogeneity in clinical cohorts using normative models: beyond case-control studies. Biol Psychiatry. 2016;80:552–61.
31. Wolfers T, Doan NT, Kaufmann T, Alnæs D, Moberget T, Agartz I, et al. Mapping the heterogeneous phenotype of schizophrenia and bipolar disorder using normative models. JAMA Psychiatry. 2018;75:1146–55.
32. Zabihi M, Oldehinkel M, Wolfers T, Frouin V, Goyard D, Loth E, et al. Dissecting the heterogeneous cortical anatomy of autism spectrum disorder using normative models. Biol Psychiatry Cogn Neurosci Neuroimaging. 2019;4:567–78.
33. Sun X, Sun J, Lu X, Dong Q, Zhang L, Wang W, et al. Mapping neurophysiological subtypes of major depressive disorder using normative models of the functional connectome. Biol Psychiatry. 2023;94:936–47.
34. Di Martino A, Yan CG, Li Q, Denio E, Castellanos FX, Alaerts K, et al. The autism brain imaging data exchange: towards a large-scale evaluation of the intrinsic brain architecture in autism. Mol Psychiatry. 2014;19:659–67.
35. Di Martino A, O'Connor D, Chen B, Alaerts K, Anderson JS, Assaf M, et al. Enhancing studies of the connectome in autism using the autism brain imaging data exchange II. Sci Data. 2017;4:170010.
36. Sun Y, Hu G, Zhang Y, Lu B, Lu Z, Fan J, et al. Eigen microstates and their evolutions in complex systems. Commun Theor Phys. 2021;73:065603.
37. Hu G, Liu T, Liu M, Chen W, Chen X. Condensation of eigen microstate in statistical ensemble and phase transition. Sci China Phys Mech Astron. 2019;62:990511.
38. Chen X, Ren H, Tang Z, Zhou K, Zhou L, Zuo Z, et al. Leading basic modes of spontaneous activity drive individual functional connectivity organization in the resting human brain. Commun Biol. 2023;6:892.
39. Zielinski BA, Prigge MB, Nielsen JA, Froehlich AL, Abildskov TJ, Anderson JS, et al. Longitudinal changes in cortical thickness in autism and typical development. Brain. 2014;137:1799–812.
40. Khundrakpam BS, Lewis JD, Kostopoulos P, Carbonell F, Evans AC. Cortical thickness abnormalities in autism spectrum disorders through late childhood, adolescence, and adulthood: a large-scale MRI study. Cereb Cortex. 2017;27:1721–31.
41. Ecker C, Pretzsch CM, Bletsch A, Mann C, Schaefer T, Ambrosino S, et al. Inter-individual differences in cortical thickness and their genomic underpinnings in autism spectrum disorder. Am J Psychiatry. 2021;179:242–54.
42. Wang J, Wang X, Xia M, Liao X, Evans A, He Y. GRETNA: a graph theoretical network analysis toolbox for imaging connectomics. Front Hum Neurosci. 2015;9:386.
43. Gaser C, Dahnke R, Thompson PM, Kurth F, Luders E, the Alzheimer's Disease Neuroimaging. Initiative. CAT: a computational anatomy toolbox for the analysis of structural MRI data. Gigascience. 2024;13:giae049.
44. Ashburner J, Friston KJ. Unified segmentation. Neuroimage. 2005;26:839–51.
45. Schaefer A, Kong R, Gordon EM, Laumann TO, Zuo X-N, Holmes AJ, et al. Local-global parcellation of the human cerebral cortex from intrinsic functional connectivity MRI. Cereb Cortex. 2018;28:3095–114.

46. Yu M, Linn KA, Cook PA, Phillips ML, McInnis M, Fava M, et al. Statistical harmonization corrects site effects in functional connectivity measurements from multi-site fMRI data. Hum Brain Mapp. 2018;39:4213–27.
47. Power JD, Barnes KA, Snyder AZ, Schlaggar BL, Petersen SE. Spurious but systematic correlations in functional connectivity MRI networks arise from subject motion. Neuroimage. 2012;59:2142–54.
48. Cattell RB. The scree test for the number of factors. Multivariate Behav Res. 1966;1:245–76.
49. Satopaa V, Albrecht J, Irwin D, Raghavan B. Finding a "kneedle" in a haystack: detecting knee points in system behavior. *2011 31st International Conference on Distributed Computing Systems Workshops*. IEEE: Minneapolis, MN, USA, 2011, pp 166-71.
50. Yeo BT, Krienen FM, Sepulcre J, Sabuncu MR, Lashkari D, Hollinshead M, et al. The organization of the human cerebral cortex estimated by intrinsic functional connectivity. J Neurophysiol. 2011;106:1125–65.
51. Rasmussen CE, Williams CKI. *Gaussian processes for machine learning*. MIT Press: Cambridge, MA, 2006.
52. Benjamini Y, Hochberg Y. Controlling the false discovery rate: a practical and powerful approach to multiple testing. J R Stat Soc Series B Stat Methodol. 1995;57:289–300.
53. Charrad M, Ghazzali N, Boiteau V, Niknafs A. NbClust: an R package for determining the relevant number of clusters in a data set. J Stat Softw. 2014;61:1–36.
54. Cohen J. *Statistical power analysis for the behavioral sciences*. (2nd ed.). Lawrence Erlbaum: Hillsdale, NJ, 1988.
55. Hotelling H. Relations between two sets of variates. Biometrika. 1935;28:321–77.
56. Dahnke R, Yotter RA, Gaser C. Cortical thickness and central surface estimation. Neuroimage. 2013;65:336–48.
57. Hong SJ, Valk SL, Di Martino A, Milham MP, Bernhardt BC. Multidimensional neuroanatomical subtyping of autism spectrum disorder. Cereb Cortex. 2018;28:3578–88.
58. Shan X, Uddin LQ, Ma R, Xu P, Xiao J, Li L, et al. Disentangling the individual-shared and individual-specific subspace of altered brain functional connectivity in autism spectrum disorder. Biol Psychiatry. 2024;95:870–80.
59. Breiman L. Random forests. Mach Learn. 2001;45:5–32.
60. Bradley AP. The use of the area under the ROC curve in the evaluation of machine learning algorithms. Pattern Recognit. 1997;30:1145–59.
61. Allen EA, Damaraju E, Plis SM, Erhardt EB, Eichele T, Calhoun VD. Tracking whole-brain connectivity dynamics in the resting state. Cereb Cortex. 2014;24:663–76.
62. Ye J, Sun H, Gao S, Dadashkarimi J, Rosenblatt M, Rodriguez RX, et al. Altered brain dynamics across bipolar disorder and schizophrenia during rest and task switching revealed by overlapping brain states. Biol Psychiatry. 2023;94:580–90.
63. Margulies DS, Ghosh SS, Goulas A, Falkiewicz M, Huntenburg JM, Langs G, et al. Situating the default-mode network along a principal gradient of macroscale cortical organization. Proc Natl Acad Sci USA. 2016;113:12574–9.
64. Hong S-J, Xu T, Nikolaidis A, Smallwood J, Margulies DS, Bernhardt B, et al. Toward a connectivity gradient-based framework for reproducible biomarker discovery. Neuroimage. 2020;223:117322.
65. Gratton C, Laumann TO, Nielsen AN, Greene DJ, Gordon EM, Gilmore AW, et al. Functional brain networks are dominated by stable group and individual factors, not cognitive or daily variation. Neuron. 2018;98:439–52.e5
66. Becht AI, Mills KL. Modeling individual differences in brain development. Biol Psychiatry. 2020;88:63–9.
67. Gao Y, Linke A, Jao Keehn RJ, Punyamurthula S, Jahedi A, Gates K, et al. The language network in autism: atypical functional connectivity with default mode and visual regions. Autism Res. 2019;12:1344–55.
68. Keehn B, Lincoln AJ, Müller RA, Townsend J. Attentional networks in children and adolescents with autism spectrum disorder. J Child Psychol Psychiatry. 2010;51:1251–9.
69. May KE, Kana RK. Frontoparietal network in executive functioning in autism spectrum disorder. Autism Res. 2020;13:1762–77.
70. Li W, Mai X, Liu C. The default mode network and social understanding of others: what do brain connectivity studies tell us. Front Hum Neurosci. 2014;8:74.
71. Oldehinkel M, Mennes M, Marquand A, Charman T, Tillmann J, Ecker C, et al. Altered connectivity between cerebellum, visual, and sensory-motor networks in autism spectrum disorder: results from the EU-AIMS longitudinal European autism project. Biol Psychiatry Cogn Neurosci Neuroimaging. 2019;4:260–70.
72. Fitzgerald J, Johnson K, Kehoe E, Bokde ALW, Garavan H, Gallagher L, et al. Disrupted functional connectivity in dorsal and ventral attention networks during attention orienting in autism spectrum disorders. Autism Res. 2015;8:136–52.
73. Rasero J, Jimenez-Marin A, Diez I, Toro R, Hasan MT, Cortes JM. The neurogenetics of functional connectivity alterations in autism: insights from subtyping in 657 individuals. Biol Psychiatry. 2023;94:804–13.
74. Zeng L-L, Wang D, Fox MD, Sabuncu M, Hu D, Ge M, et al. Neurobiological basis of head motion in brain imaging. Proc Natl Acad Sci USA. 2014;111:6058–62.
75. Shi TC, Durham K, Marsh R, Pagliaccio D. Differences in head motion during functional magnetic resonance imaging across pediatric neuropsychiatric disorders. Biol Psychiatry Glob Open Sci. 2025;5:100446.
76. Pardoe HR, Kucharsky Hiess R, Kuzniecky R. Motion and morphometry in clinical and nonclinical populations. Neuroimage. 2016;135:177–85.
77. Hardan AY, Muddasani S, Vemulapalli M, Keshavan MS, Minshew NJ. An MRI study of increased cortical thickness in autism. Am J Psychiatry. 2006;163:1290–2.
78. Wallace GL, Dankner N, Kenworthy L, Giedd JN, Martin A. Age-related temporal and parietal cortical thinning in autism spectrum disorders. Brain. 2010;133:3745–54.
79. Valk SL, Di Martino A, Milham MP, Bernhardt BC. Multicenter mapping of structural network alterations in autism. Hum Brain Mapp. 2015;36:2364–73.
80. Zabihi M, Floris DL, Kia SM, Wolfers T, Tillmann J, Arenas AL, et al. Fractionating autism based on neuroanatomical normative modeling. Transl Psychiatry. 2020;10:384.
81. Liang X, Sun L, Xia M, Zhao T, Gong G, Li Q, et al. Dissecting human cortical similarity networks across the lifespan. Neuron. 2025;113:3275–95.e11
82. Huttenlocher PR. Synaptic density in human frontal cortex - developmental changes and effects of aging. Brain Res. 1979;163:195–205.
83. Natu VS, Gomez J, Barnett M, Jeska B, Kirilina E, Jaeger C, et al. Apparent thinning of human visual cortex during childhood is associated with myelination. Proc Natl Acad Sci USA. 2019;116:20750–9.
84. Lord L-D, Stevner AB, Deco G, Kringelbach ML. Understanding principles of integration and segregation using whole-brain computational connectomics: implications for neuropsychiatric disorders. Philos Trans A Math Phys Eng Sci. 2017;375:20160283.
85. Deco G, Kringelbach ML. Great expectations: using whole-brain computational connectomics for understanding neuropsychiatric disorders. Neuron. 2014;84:892–905.
86. Tavares V, Fernandes LA, Antunes M, Ferreira H, Prata D. Sex differences in functional connectivity between resting state brain networks in autism spectrum disorder. J Autism Dev Disord. 2022;52:3088–101.
87. Lawrence KE, Hernandez LM, Bowman HC, Padgaonkar NT, Fuster E, Jack A, et al. Sex differences in functional connectivity of the salience, default mode, and central executive networks in youth with ASD. Cereb Cortex. 2020;30:5107–20.
88. Li C, Li T, Chen Y, Zhang C, Ning M, Qin R, et al. Sex differences of the triple network model in children with autism: a resting-state fMRI investigation of effective connectivity. Autism Res. 2023;16:1693–706.
89. Ma XE, Belmonte MK, Zhao Y, Zhao J. Sex similarities and differences in brain dynamic functional connectivity among individuals with and without autism spectrum disorders. Hum Brain Mapp. 2025;46:e70423.
90. Buch AM, Vértes PE, Seidlitz J, Kim SH, Grosenick L, Liston C. Molecular and network-level mechanisms explaining individual differences in autism spectrum disorder. Nat Neurosci. 2023;26:650–63.
91. O'Connell ME, Kadlec H, Griffith LE, Maimon G, Wolfson C, Taler V, et al. Methodological considerations when establishing reliable and valid normative data: canadian longitudinal study on aging (CLSA) neuropsychological battery. Clin Neuropsychol. 2022;36:2168–87.
92. Berthet P, Haatveit BC, Kjelkenes R, Worker A, Kia SM, Wolfers T, et al. A 10-year longitudinal study of brain cortical thickness in people with first-episode psychosis using normative models. Schizophr Bull. 2025;51:95–107.
93. Wiggins LD, Reynolds A, Rice CE, Moody EJ, Bernal P, Blaskey L, et al. Using standardized diagnostic instruments to classify children with autism in the study to explore early development. J Autism Dev Disord. 2015;45:1271–80.
94. Hus Y, Segal O. Challenges surrounding the diagnosis of autism in children. Neuropsychiatr Dis Treat. 2021;17:3509–29.
95. Litman A, Sauerwald N, Green Snyder L, Foss-Feig J, Park CY, Hao Y, et al. Decomposition of phenotypic heterogeneity in autism reveals underlying genetic programs. Nat Genet. 2025;57:1611–9.
96. Bush G. Attention-deficit/hyperactivity disorder and attention networks. Neuropsychopharmacol. 2010;35:278–300.
97. Hahamy A, Behrmann M, Malach R. The idiosyncratic brain: distortion of spontaneous connectivity patterns in autism spectrum disorder. Nat Neurosci. 2015;18:302–9.
98. Khushboo, Siddiqi NJ, de Lourdes Pereira M, Sharma B. Neuroanatomical, biochemical, and functional modifications in brain induced by treatment with antidepressants. Mol Neurobiol. 2022;59:3564–84.
99. Xia M, Wang J, He Y. BrainNet viewer: a network visualization tool for human brain connectomics. PLoS ONE. 2013;8:e68910.

ACKNOWLEDGEMENTS

We thank Dr. Xiaoyi Sun for valuable discussion.

AUTHOR CONTRIBUTIONS

THL and XHL designed the research; XC, HDR, LY, YH, and XHL provided the methodological instruction; XYZ, ZF, YLZ, and LY collected the PKUSH dataset; THL and YPX performed the data analysis; THL and XHL wrote the paper; THL, YH, LY, and XHL revised the paper.

FUNDING

This work was supported by the National Natural Science Foundation of China (Grant Nos. 81971690, 82021004, and 11835003), Beijing Natural Science Foundation (Grant No. 5262012), and the Tang Scholar Award of Beijing Normal University.

COMPETING INTERESTS

The authors report no biomedical financial interests or potential conflicts of interest.

ADDITIONAL INFORMATION

Supplementary information The online version contains supplementary material available at https://doi.org/10.1038/s41380-026-03627-y.

Correspondence and requests for materials should be addressed to Li Yang, Yong He or Xuhong Liao.